




The fretting tribocorrosion properties of CrAlTiN coating on the Inconel 690 alloy

Xiaohui Kang¹, Hui Qiu¹, Guizhong Li^{1,2}, and Meigui Yin^{1,2,*} 

¹College of Mechanical and Electrical Engineering, Wenzhou University, Wenzhou 325035, China

²Wenzhou University Pingyang Institute of Intelligent Manufacturing, Wenzhou 325400, China

Received: 29 December 2022

Accepted: 17 March 2023

Published online:

4 April 2023

© The Author(s), under exclusive licence to Springer Science+Business Media, LLC, part of Springer Nature 2023

ABSTRACT

The fretting tribocorrosion resistance of steam generator tubes essentially affects on the pressurized water reactor power plant's safety and stable operation. In this study, a high-performance CrAlTiN coating deposited by plasma spraying technique on the surface of an Inconel 690 alloy tube was fabricated, and its fretting wear and electrochemical corrosion behaviors were investigated. Although the CrAlTiN coating's surface compressive residual stress is lower than the Inconel 690 alloy tube, its more excellent surface nano-hardness and elastic modulus help reduce the tribocorrosion degree of the treated alloy tubes. In addition, this coating decreased the friction coefficient. Electrochemical corrosion tests show that the corrosion rate was reduced by the CrAlTiN coating, and an increased normal load would accelerate the corrosion degree. Moreover, the primary tribocorrosion mechanism includes pitting corrosion, abrasive, and oxidation wear.

Introduction

Fretting tribocorrosion is always derived from the simultaneous action of the chemical, electrochemical, and mechanical, thus resulting in a degradation of materials in fretting contact modes under corrosion conditions [1]. Inner the steam generators of nuclear pressurized water reactors, with the turbulent buffeting, Strouhal periodicity, and fluid elastic instability excitation mechanisms in place, led to the fretting wear behaviors commonly occur between

steam generator tubes and their support plates [2]. Furthermore, desalting and boracic seawater that served as coolants are corrosive, thus making fretting wear and corrosion simultaneously happening, that is, fretting tribocorrosion. Approximately 40% of abnormal shutdown accidents in nuclear reactors were caused by the fretting tribocorrosion failure of steam generator tubes [3].

Fretting tribocorrosion belongs to a complicated dynamic damage process that is affected by the coupling effect of various mechanical, environmental, and material factors. Major mechanical parameters

Handling editor: Catalin Croitoru .

Address correspondence to E-mail: 1148129987@qq.com

<https://doi.org/10.1007/s10853-023-08403-9>

refer to normal load, displacement amplitude, and fretting frequency. Liao and Li et al. concluded that the normal load would significantly affect the initiation and propagation mechanism of fretting corrosion fatigue cracks of Inconel 690 alloy [4, 5]. Meanwhile, Zhang and Xin et al. found that the increased fretting frequency would accelerate the removal of the ultra-fine grained wear debris and aggravates the plastic deformation of the nanostructured TTS layer, which finally exacerbates fretting corrosion [6, 7]. Xin reveals in detail the formation and metastasis of oxide in the fretting corrosion process of the Inconel 690 TT alloy in high-temperature and high-pressure pure water under partial slip conditions [8]. However, the real working condition of nuclear steam generator tubes is very complex and rigorous. Environmental factors such as temperature, pH, dissolved oxygen or hydrogen, and impurity concentrations of coolant could affect the fretting corrosion behavior of steam generator tubes. Liu found that the fretting corrosion degree of alloy 690 TT under 100 °C water is higher than the level of room temperature or 200 °C [9]. The pH value of the coolant mostly depends on the content of impurities, and extremely acidic or alkaline conditions would aggravate corrosion problems in steam generator tubes [2, 10]. Moreover, according to Xin et al., the changes to the dissolved oxygen will affect the competition between the surface film rupture rate, re-passivation rate, and the initiation of corrosion fatigue cracks [11]. Abnormal amounts of some impurities such as chloride, magnetite, zinc, and ferrite can negatively affect the composition and structure of corrosion oxidation film [12–14]. As for the material factors, pieces of the literature can be indexed primarily because steam generator tubes belong to nuclear grade material, and there are very limited types applied to the engineering practice [15].

In general, the corrosion behavior of steam generator tubes is accompanied by an electrochemical process. From this, electrochemical techniques have been widely applied to characterize the corrosion dynamic behavior of the alloy tube in the active, passive, and trans-passive states, including the corrosion rate, polarization resistance, and corrosion mechanism [16]. In virtue of the electrochemical technique, Peraud et al. revealed the dissolution kinetics and passivation tendency of alloy 600 and alloy 800 under acid sulfate solutions at 315 °C [17]. Meanwhile, Betova investigated how the addition of

lead affects the electrochemical behavior of the alloy 690 tube in acidic and alkaline crevice solutions at 278 °C [18]. Furthermore, Wang and Li et al. applied high-temperature and pressure in situ electrochemical technology to reveal how the temperature variables affect the corrosion dynamic behaviors of the 690 alloy [19, 20]. Each also revealed how the oxidation properties of alloy 690 surface influenced its electrochemical behaviors under simulated service conditions [21]. Thus, an in-depth study of the corrosion behaviors of steam generator tubes is important for nuclear power plants because corrosion failure may cause several serious problems [10].

Herein, several surface intensity technologies such as ultrasonic surface rolling process [22, 23], shot peening [24], and localized heat treating [25] have been investigated to further improve the surface tribocorrosion resistance of steam generator tubes. In addition, surface coating technology has been widely applied to create a different thin-film material on the substrate to enhance some of its service properties. Given that CrAlTiN coatings have the advantages of excellent hardness, toughness, wear resistance, anti-oxidation, and fatigue strength, it has been widely applied in transportation, aviation, and petrochemical fields [26–28].

Considering the excellent quality of the CrAlTiN coating, this study applied specific magnetron sputtering technology to fabricate CrAlTiN coatings on the outer surface of the Inconel 690 alloy tube. Then, with the help of a self-made fretting tribocorrosion test rig, it is investigated how this coating influences the fretting wear mechanism and electrochemical corrosion performances of the Inconel 690 alloy tube in 3.5% NaCl solution.

Moreover, open circuit potential (OCP), potentiodynamic polarization (PP), and electrochemical impedance spectroscopy (EIS) were analyzed to comparatively evaluate the electrochemical corrosion properties of both substrate and coating-treated alloy tubes. Furthermore, fretting failure behaviors, wear interface dynamic response, and dissipated friction energy of all test samples were studied.

Experimental procedures

Substrate materials

The as-received Inconel 690 alloy tube was made by the Zhejiang JiuLi Hi-Tech Metals Co., Ltd. The nominal chemical composition of this base alloy tube is approximately: C 0.0258%, Cr 27.33%, Fe 9.66%, Ni 50.76%, and some trace elements. The specification of all tested tubes was set as follows: external diameter, thickness, and length of 17.48, 1.01, and 10 mm, respectively. In addition, the substrate should be mirror polished and ultrasonically cleaned with ethanol before being used.

Coating preparations

High vacuum magnetron, the sputtering process, has the advantage to precisely controlling the composition, thickness, homogeneity, and mechanical properties of deposited coatings [29]. In this study, the spraying process was performed in the MDP650 magnetron sputtering vacuum ion plating system which adopts pure metallic targets. The alloy tubes that need to be sprayed were fixed at a table that rotates at 5 rpm. Then, nitrogen was introduced into the system to form nitride coatings with evaporated cathode materials, and the argon gases with a constant flow rate of approximately 20 sccm were applied to maintain a stable working pressure of about 0.17 Pa. Subsequently, further surface preparation was carried out by preheating the substrates to 550 °C, and sputter cleaning with Ar⁺ plasma was performed inside the vacuum chamber for 30 min. After reducing the base pressure to approximately 1.33×10^{-3} Pa, the substrates were biased with a pulsed direct current voltage of – 500 V with a frequency of 250 kHz. A thin Cr bond layer was deposited during deposition, followed by a thin CrN layer and then a compositionally graded CrAl-TiN layer.

Fretting tribocorrosion tests

All the experimental tests were performed on a fretting tribocorrosion test rig, as shown in Fig. 1. The working principle of this rig can be referred to [23]. Meanwhile, the specific fretting parameters of this study are exhibited in Table 1. Furthermore, the Al₂O₃ ceramic column (length: 10 mm and diameter:

10 mm) was selected as the up-friction pair to ensure the electrochemical corrosion test results are accurate and reliable. During the fretting process, the alloy tube was fixed on a jig and reciprocating sliding under the drive of voice coil motor. Normal load was applied through the static up-friction pair.

All electrochemical measurements were carried out through a ChenHua CHI600E-650E electrochemical workstation, and the electrolyte was an aqueous 3.5% NaCl solution (pH ≈ 8.98). The measurements were made in the conventional three-electrode cell, in which saturated calomel was employed as the reference electrode, the counter electrode was a platinum plate, and a working electrode of the sample was connected to a leading wire and then mounted with resin, thereby leaving an exposed working circle area with a diameter of approximately 2 mm. In addition, the polarization curves were measured from the corrosion potential (E_{corr}) in cathodic and anodic directions, with a scan rate of 0.5 mV/s. The electrochemical impedance spectroscopy (EIS) measurements were performed at OCP with a frequency range from 10^5 to 0.01 Hz using a 10-mV amplitude sinusoidal voltage. Moreover, each experiment test was repeated thrice to ensure the accuracy and repeatability of all test results.

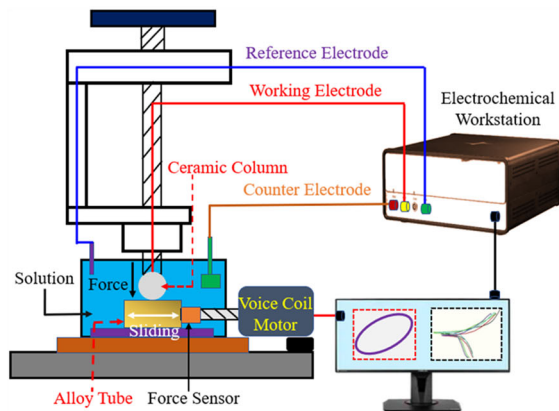
Characterization methods

In this study, the microstructure and chemical composition of all test samples and fretting tribocorrosion scars were observed using scanning electron microscopy equipped with an energy dispersive X-ray spectrometer (Nova 200 NanoSEM). The phase characterization of all test samples was measured by XRD (Bruker D8 Advance). The wear volume and depth of all worn scars were characterized by a white-light interferometer (Bruker Contour GT-1 Germany).

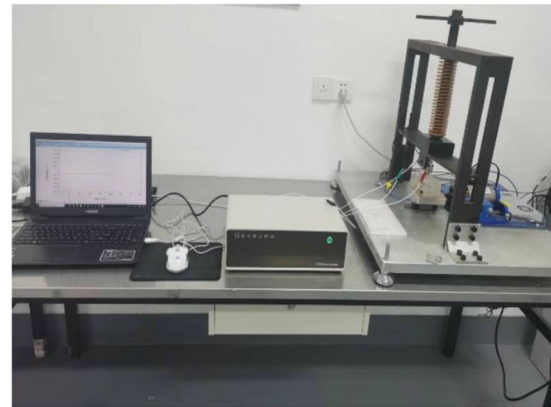
Results

Characterization of samples

The surface morphology, EDX graph, XRD pattern, and cross-sectioned CrAlTiN coating are expressed in Fig. 2. In general, the coating surface looks pretty dense; however, there are various irregular distributions of large particles, pits, and micro-cracks (Fig. 2a). These large particles were primarily caused



(a) Schematic diagram



(b) Physical map

Figure 1 Fretting tribocorrosion test rig.**Table 1** Parameters of the fretting tribocorrosion test

Item	Values
Test samples	Substrate, coating-treated
Sliding displacement	200 μm
Fretting frequency	20 Hz
Temperature	RT, air condition
Normal load	30 N, 60 N
Fretting time	3 h

by the high-temperature energetic ion bombardment on the growing coating. The pits are induced by the debonding of poorly adhered metal particles. Given the shrinkage behavior of deposited coatings, tensile stresses are existed, thereby leading to some micro-cracks that formed among the loosely bounded droplets detached from the coating [30]. Furthermore, the thickness of the sprayed coating is approximately 8 μm , and it displayed perfect bonding performance with the substrate (Fig. 2b).

The chemical compositions of the CrAlTiN coating measured from the surface are presented in Fig. 2c. A certain amount of Cr was observed in this coating ($\sim 65.2\%$ wt%). The primary diffraction peaks of the nanolayered CrAlTiN coating primarily belonged to the (111), (101), (200), (220), and (312) crystalline planes, and the corresponding chemical compositions were AlTiC, CrN, CrFeNi, TiO, and TiN, respectively (Fig. 2d).

Figure 3 exhibits some surface mechanical properties of both substrate and CrAlTiN coating-treated samples. Meanwhile, indentation loading curves of both the substrate and coating-treated alloy tubes are

exhibited in Fig. 3a. The load–depth plot of the CrAlTiN coating-treated sample is smooth, which indicates that the coating's surface is dense and uniform to some extent. The maximum penetration depth of the untreated alloy tube is approximately 550 nm, then about 350 nm for the coating-treated sample. The surface nano-hardness of the Inconel 690 alloy tube was improved from around 4.36–15.81 GPa after the coating was treated. This improved hardness is primarily attributed to the existence of some nano-scale grains which could impede the dislocation movements effectively. However, its residual compressive stress decreased from approximately 962.69 to 512.91 MPa after the coating was treated. The coating's residual stress was generated primarily by the peening effect of coating particles, and it was always affected by various factors such as deposition condition, spraying thickness, and material properties [31].

Fretting wear behavior

The optical micrographs of all worn scars are exhibited in Fig. 4. The wear area increased with the normal load, and the worn scar for the substrate sample is bigger than that of the CrAlTiN coating-treated sample when suffered the same normal load. This indicates that the fretting tribocorrosion resistance had been improved by the CrAlTiN coating. The surface hardness and elastic modulus of the material are key properties to assess its fretting wear behavior, and these improved properties could help optimize wear resistance. In addition, the worn area of the coating-treated samples is brighter and smoother

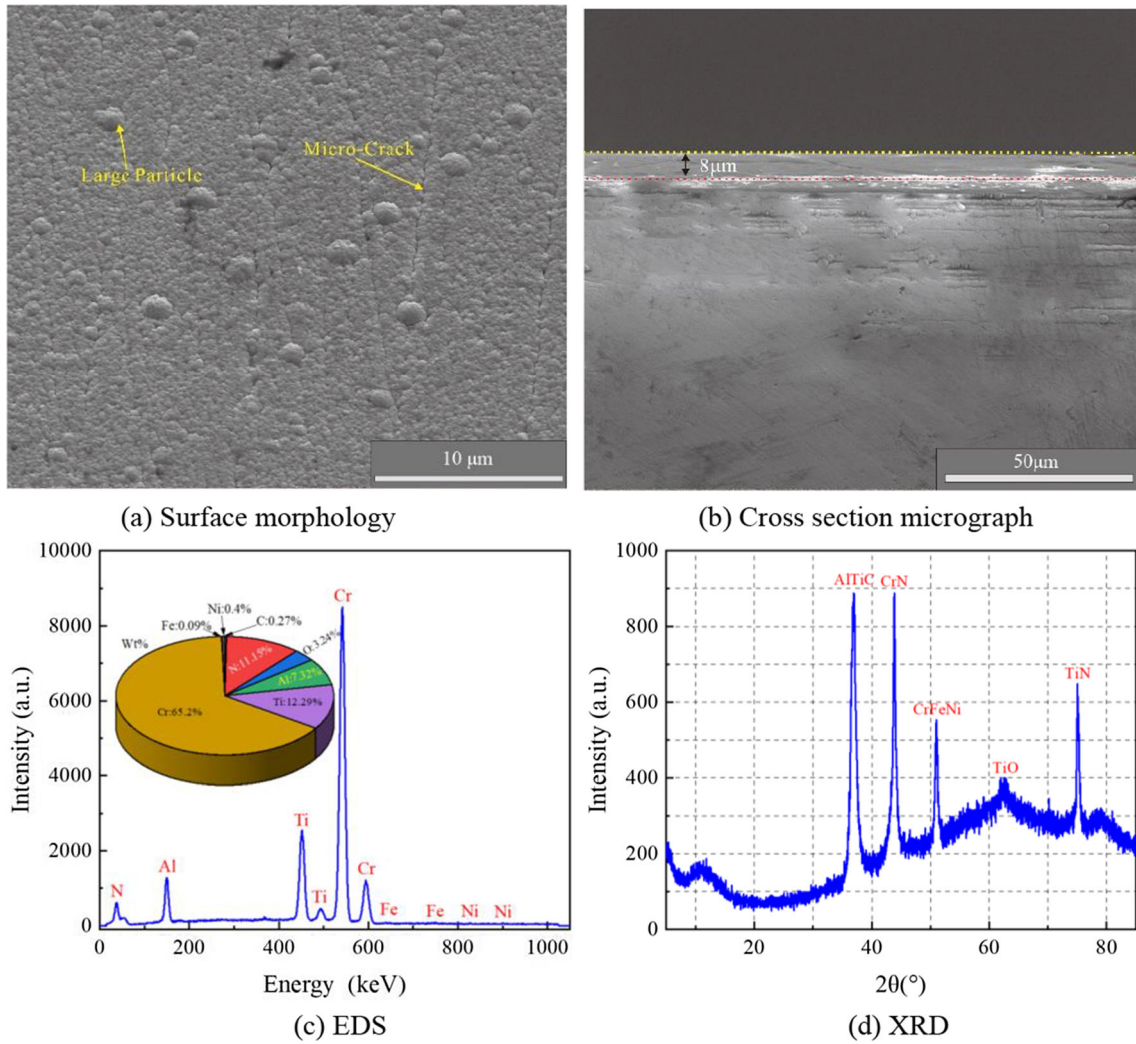


Figure 2 SEM micrographs a and b, EDS c, and XRD d of the coating sample.

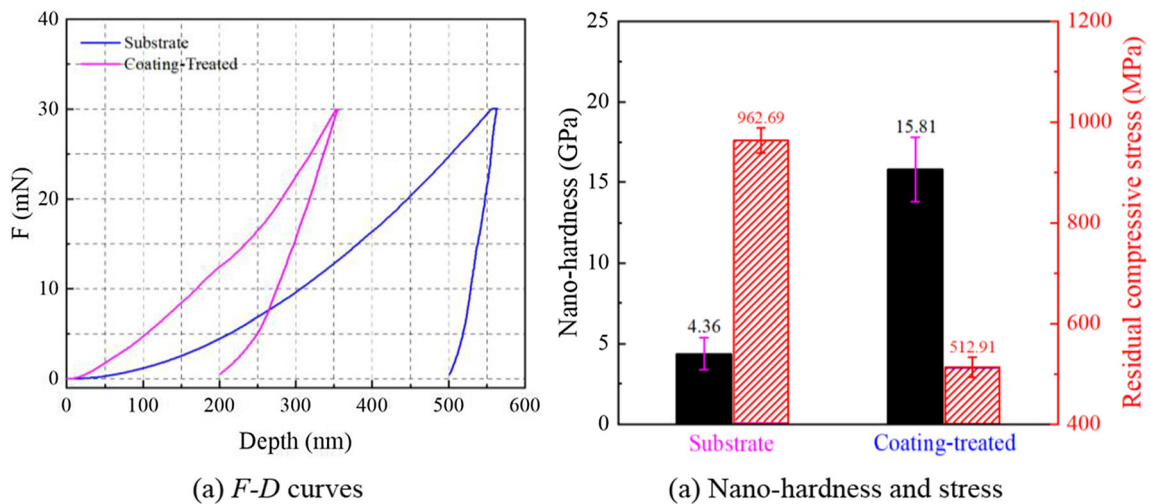


Figure 3 Mechanical properties of test samples.

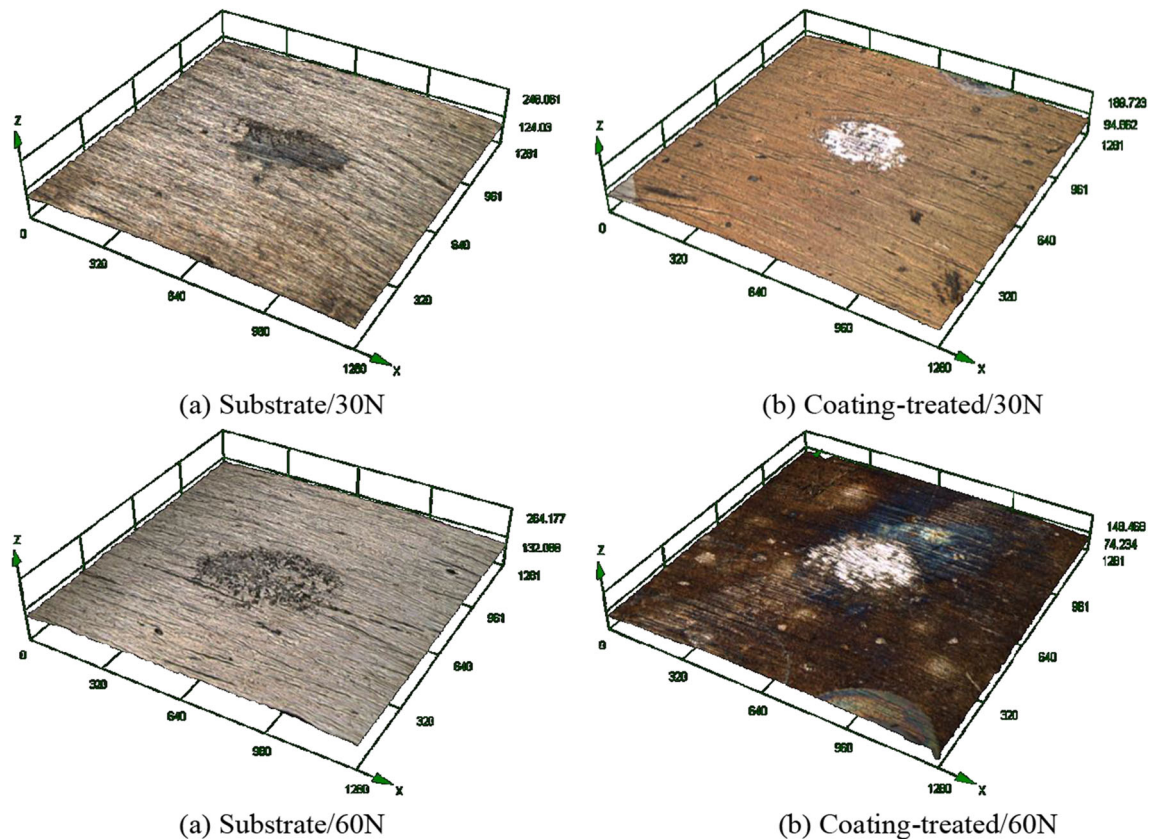


Figure 4 Optical graphs of worn scars.

than that of the blank Inconel 690 alloy tube. Thus, the oxidation reaction for the base alloy tube is more serious than that of the coating-treated sample. Danek et al. pointed out that the increased content of the Cr element could enhance the material's oxidation resistance [32]. Herein, the Cr content in the CrAlTiN coating is higher than that of the blank Inconel 690 alloy tube.

Figure 5 illustrates the fretting tribocorrosion data for the friction coefficient defined as the measured maximum tangential friction force during each sliding cycle divided by the constant normal load. In general, the friction coefficient increased at the initial stage of the fretting test and then entered a steady but fluctuated slightly state. When the normal load was 30 N, the average friction coefficients of the blank alloy tube and CrAlTiN coating-treated alloy tube were approximately 0.328 and 0.227, respectively, and these values changed to about 0.204 and 0.142 as the normal load increased to 60 N. The coating's wear-resistant phases such as CrN and TiN can improve its fretting performance and decrease the friction coefficient [28].

Herein, wear volume and depth of the worn scar are important features of test samples' fretting tribocorrosion resistance. The average wear volume and maximum wear depth of each worn scar are presented in Fig. 6. When the normal load was 30 N, the maximum wear depth of the substrate and CrAlTiN coating-treated samples were approximately 7.14 and 3.83 μm , and the corresponding wear volume was about 9.7×10^6 and $5.3 \times 10^6 \mu\text{m}^3$, respectively (Fig. 6a). Meanwhile, the maximum wear depth of the substrate and CrAlTiN coating-treated samples are increased to approximately 12.45 and 6.89 μm as the normal load increased to 60 N, and the corresponding wear volume was increased to $\sim 19.3 \times 10^6 \mu\text{m}^3$ and $12.5 \times 10^6 \mu\text{m}^3$, respectively (Fig. 6b). All these values provide further explanations of the strengthening effects of CrAlTiN coating on the fretting tribocorrosion behavior of the Inconel 690 alloy tube.

The microtopography of each test sample's worn center area was observed to further understand the tribocorrosion failure mechanism of all test samples, as shown in Fig. 7. There were evident ploughing

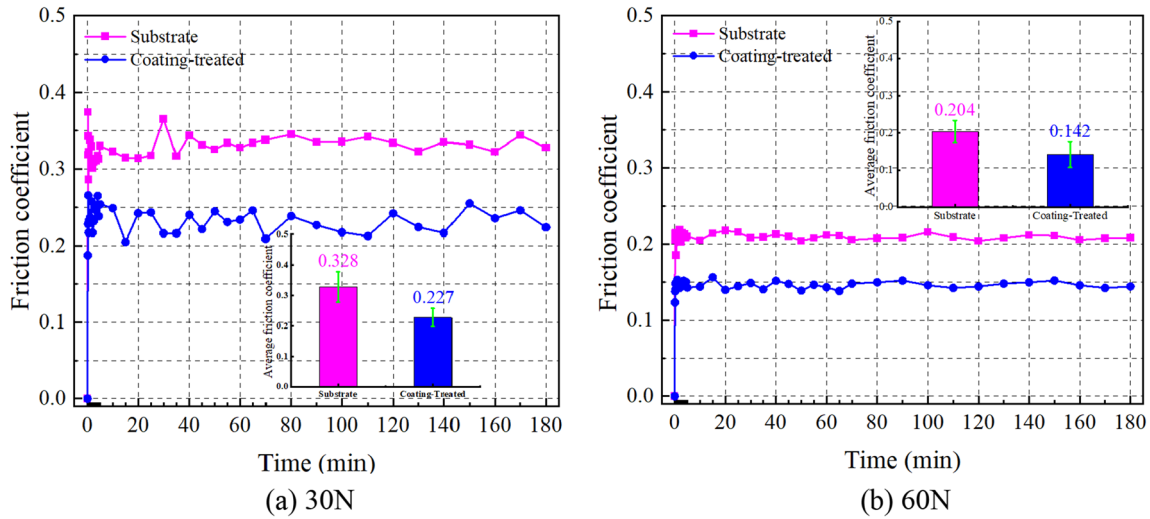


Figure 5 Friction coefficient versus fretting time.

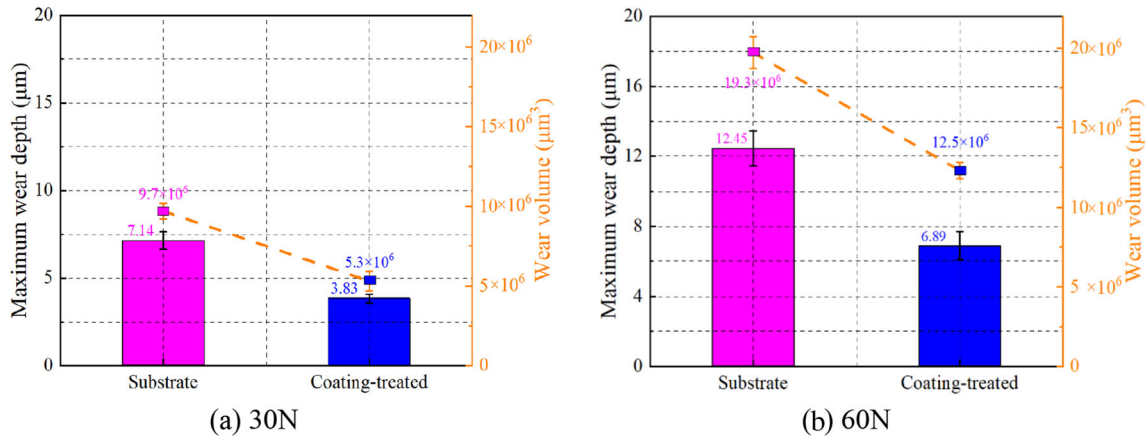


Figure 6 Wear volume and maximum wear depth of worn scars.

among all worn surfaces, thereby indicating that the tribocorrosion behaviors were dominated by mechanical wear. The test samples of the blank Inconel 690 alloy tube presented craters, with evident plastic deformation, surface delamination, and adhesion. Meanwhile, for the CrAlTiN coating-treated samples, numerous peeling pits and wear particles existed because of their semi-brittle property. Some lamellar structures also appeared, this phenomenon was primarily induced by the synergy effect between wear and sea water corrosion. The worn surface that was damaged by friction force would lead to more sea water immersed into the interior of the coating or the Inconel 690 alloy tube.

In addition, the fretting wear tracks of the substrate tubes were smoother than that of the CrAlTiN coating-treated alloy tubes. It is because the surface of the

Inconel 690 alloy tube is softer than the coating, thereby leading to their contact extent with the up-friction pair has become tight. Moreover, the worn surfaces that formed under the 60 N normal load are more distinct than that of the 30 N normal load.

EDS mapping was applied to analyze the distribution of several typical elements in the worn center area, as shown in Fig. 8. The content of oxygen for the substrate is higher than that of the CrAlTiN coating-treated samples, and a higher normal load would increase this content. The distribution of Fe and Ni elements on the substrate surface is relatively uniform (Fig. 8a and c), and for the coating-treated test sample is the Cr element (Fig. 8b and d). In addition, both Fe and Ni elements have been measured on the CrAlTiN coating-treated test samples, this is primarily caused by the wear of the coating.

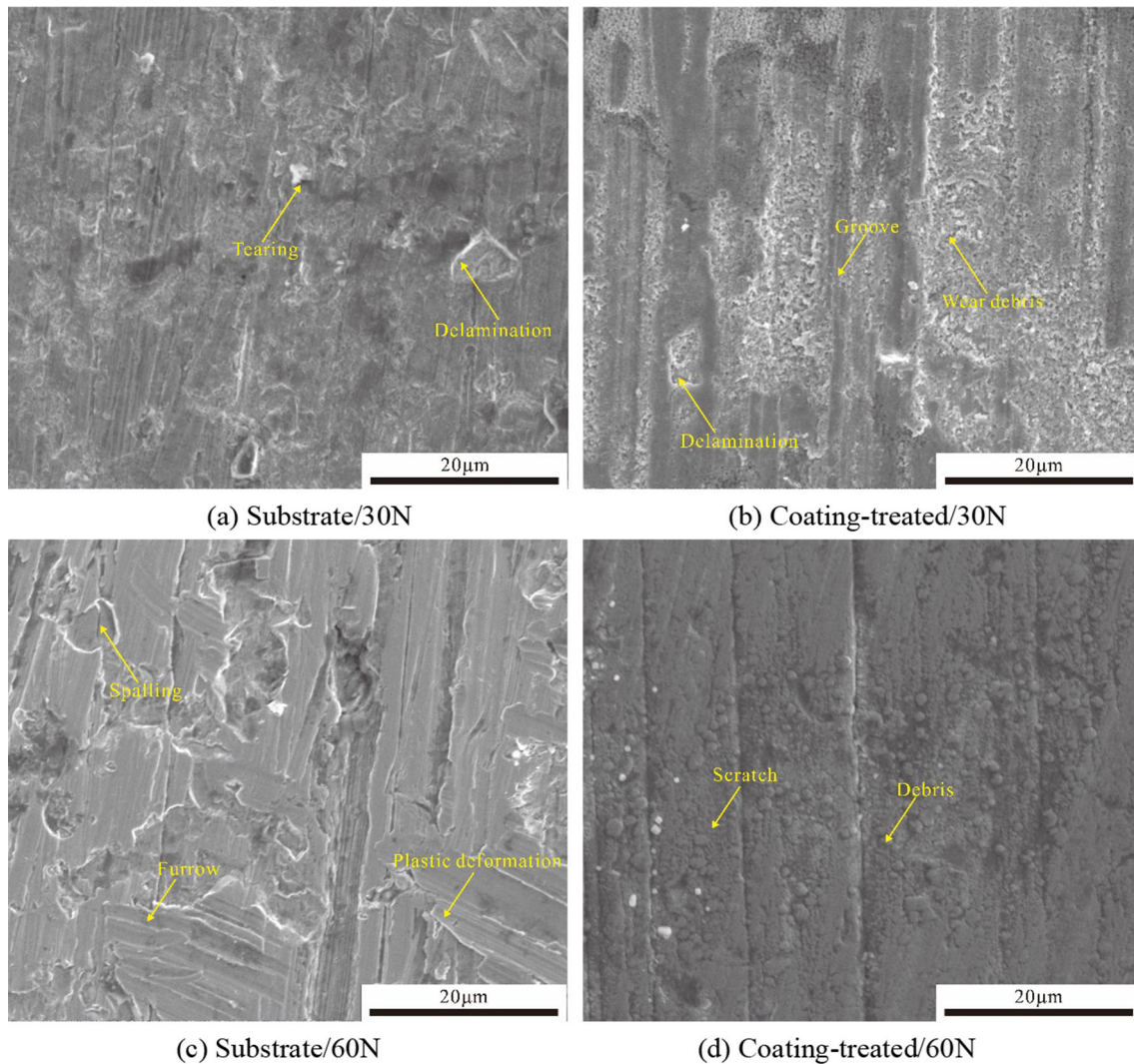


Figure 7 Micro-failure mechanism of worn scars.

Electrochemical corrosion behavior

Figure 9 exhibits the open circuit potential (OCP) versus time response curves of all test samples under various fretting conditions. The OCP was often applied to reflect the thermodynamic stability that was the oxidation tendency of the tribocorrosion surface. The thickness and the composition of the fretting oxide films are always a complex dynamic process because of the evolution behavior of the microstructure; hence, the curve of OCP may fluctuate. The increment of the potential was primarily because of the formation of passive film on the tribocorrosion surface, and the broken of the oxide layer would decrease this potential [33]. Therefore, in this study, the testing process was divided into three

phases: initial immersion (1000 s), fretting tribocorrosion test (3 h), and post-test immersion (1000 s). During the phase of fretting tribocorrosion, the sample surface suffered mechanical abrasion and formed oxide film was removed, leading to the decrease in OCP. Moreover, the OCP signals for coating-treated test samples were smoother than that of the substrates, thereby indicating that the CrAlTiN coating would enhance its self-lubricity through anti-wear performance.

Furthermore, the OCP values of the coating-treated test samples are higher than that of the substrate, this indicates that the thermodynamics resistance and inert behavior to corrosion of the CrAlTiN coating are more pronounced than the Inconel 690 alloy.

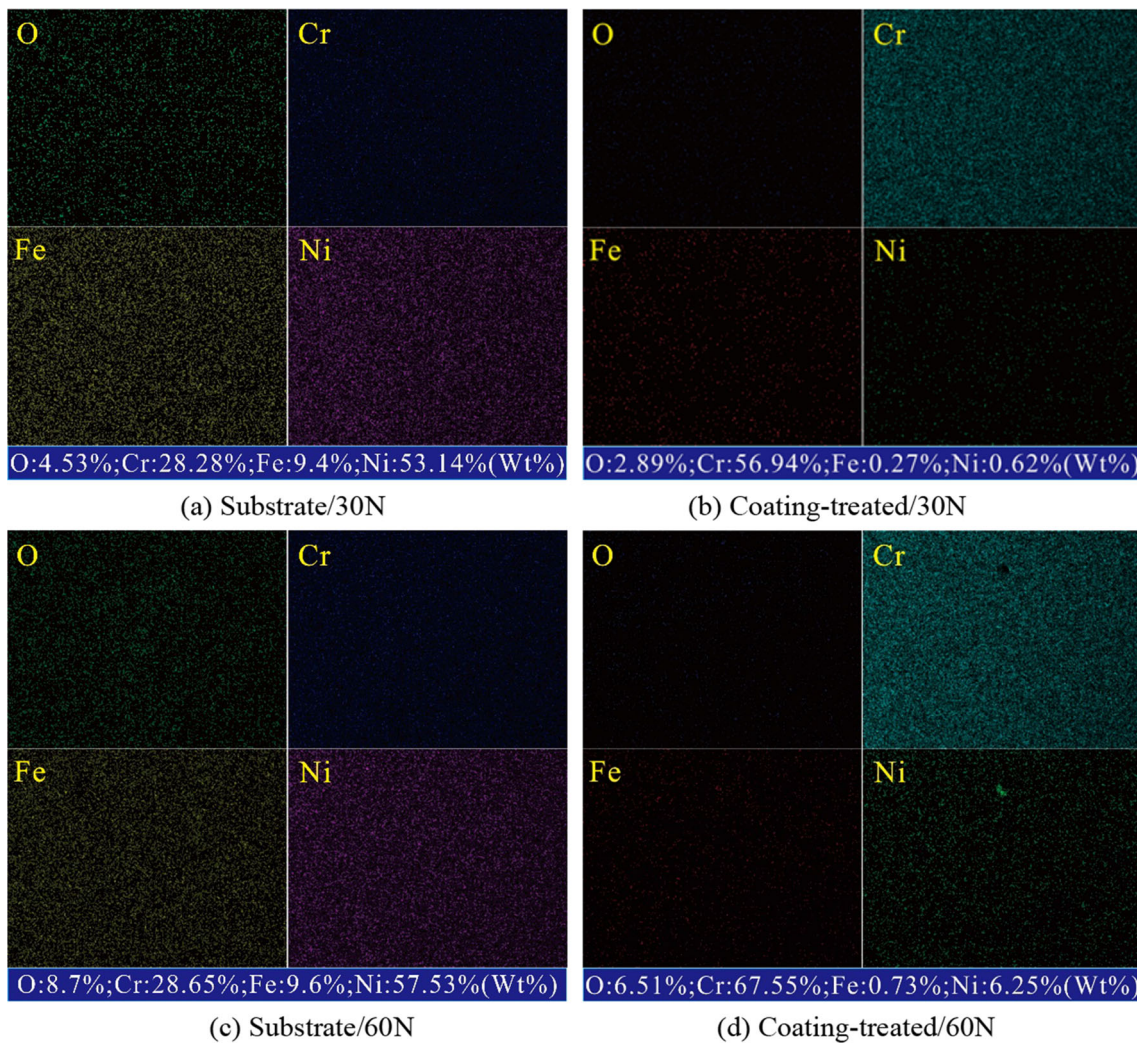


Figure 8 EDS analysis on fretting tribocorrosion scars.

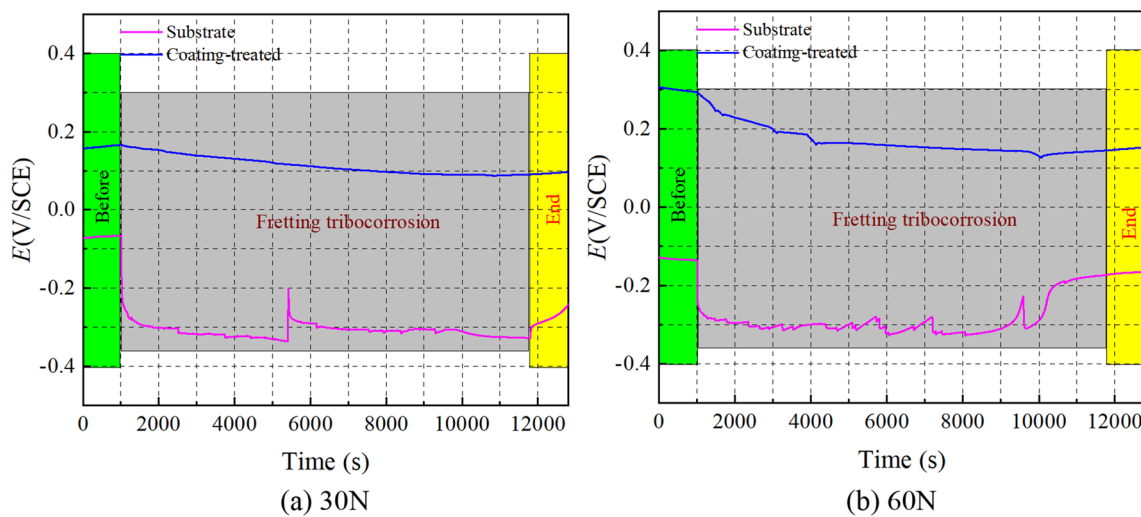


Figure 9 Variation of time of the OCP for test samples.

The typical potentiodynamic polarization curves for all test samples under various fretting tribocorrosion conditions are displayed in Fig. 10. The passive region could be found among all test samples, thereby indicating that stable oxide films have formed. The breakdown potential of the coating-treated samples is always higher than that of the substrate samples, thereby indicating that the passive film that formed on the substrate sample surface is easier to destroy, and its local corrosion resistance is poorer than that of the CrAlTiN coating-treated test samples.

Under the static condition, the corrosion current (I_{corr}) of the coating-treated sample is bigger than the substrate, that is, the corrosion rate of the CrAlTiN coating-treated sample is higher than the untreated Inconel 690 alloy tube. This is primarily because the inherence coating defects, such as droplets, porosity, and low compressive residual stress, cannot be easily avoided. Hence, this would produce a potential difference between the noble coating and the substrate, and, finally, accelerate the localized or galvanic corrosion behaviors of alloy tubes [34].

However, the corrosion current of the substrate alloy tube becomes higher than the coating-treated samples when the normal load was 30 N or 60 N. The CrAlTiN coating had better wear resistance than the substrate, less worn area, and smaller surface damage would exist than the substrate Inconel 690 alloy tube. This coating serves as a barrier layer to prevent the diffusion of the electrolyte into the substrate, thereby retarding the corrosion behaviors.

Furthermore, Nyquist plots of both substrate and CrAlTiN coating-treated Inconel 690 alloy tubes that are obtained under different fretting conditions are

displayed in Fig. 11. The curves of all test samples show a similar shape, thus exhibiting a large and incomplete capacitive semicircle, and Warburg impedance appeared, thereby indicating that the electrochemical corrosion behavior in the fretting process is primarily controlled by a moderate diffusion transfer reaction. The bigger diameter of the plot describes a more stable and thicker protective passive film on the tribocorrosion surface. Regardless of whether in static, 30 N or 60 N fretting conditions, the coating-treated alloy tube’s Nyquist semicircle diameter is bigger than that of the blank alloy tube. This indicates improved fretting tribocorrosion resistance of the tube’s surface by CrAlTiN coating.

In addition, the terminate impedance values of the substrate samples are lower than that of the coating-treated alloy tubes, thereby suggesting that the corrosion product may not deposit on the base alloy tube’s surface.

The bode plot that measured the resistance and phase versus the logarithm of the frequency for all test samples is exhibited in Fig. 12. In general, each bode diagram can roughly be divided into three stages [35]. Herein, the impedance at the high-frequency region is applied to describe how the electrolyte influences the passivation films, and the impedance at low frequency represents the protective efficiency or corrosion resistance of the interfaces. In this study, the module of the impedance of the CrAlTiN coating-treated samples is much higher than the substrate in the low-frequency region, thus representing the excellent polarization resistance of this coating. In the low-frequency region (about from 0.01–1 Hz), there is a linear relationship found between the impedance and log frequency, thereby

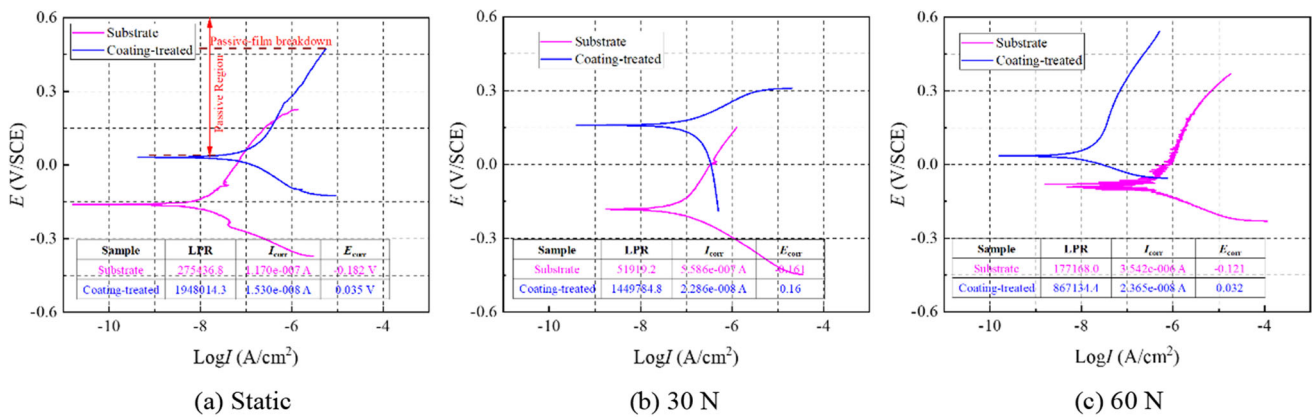


Figure 10 Potentiodynamic polarization curves for all test samples.

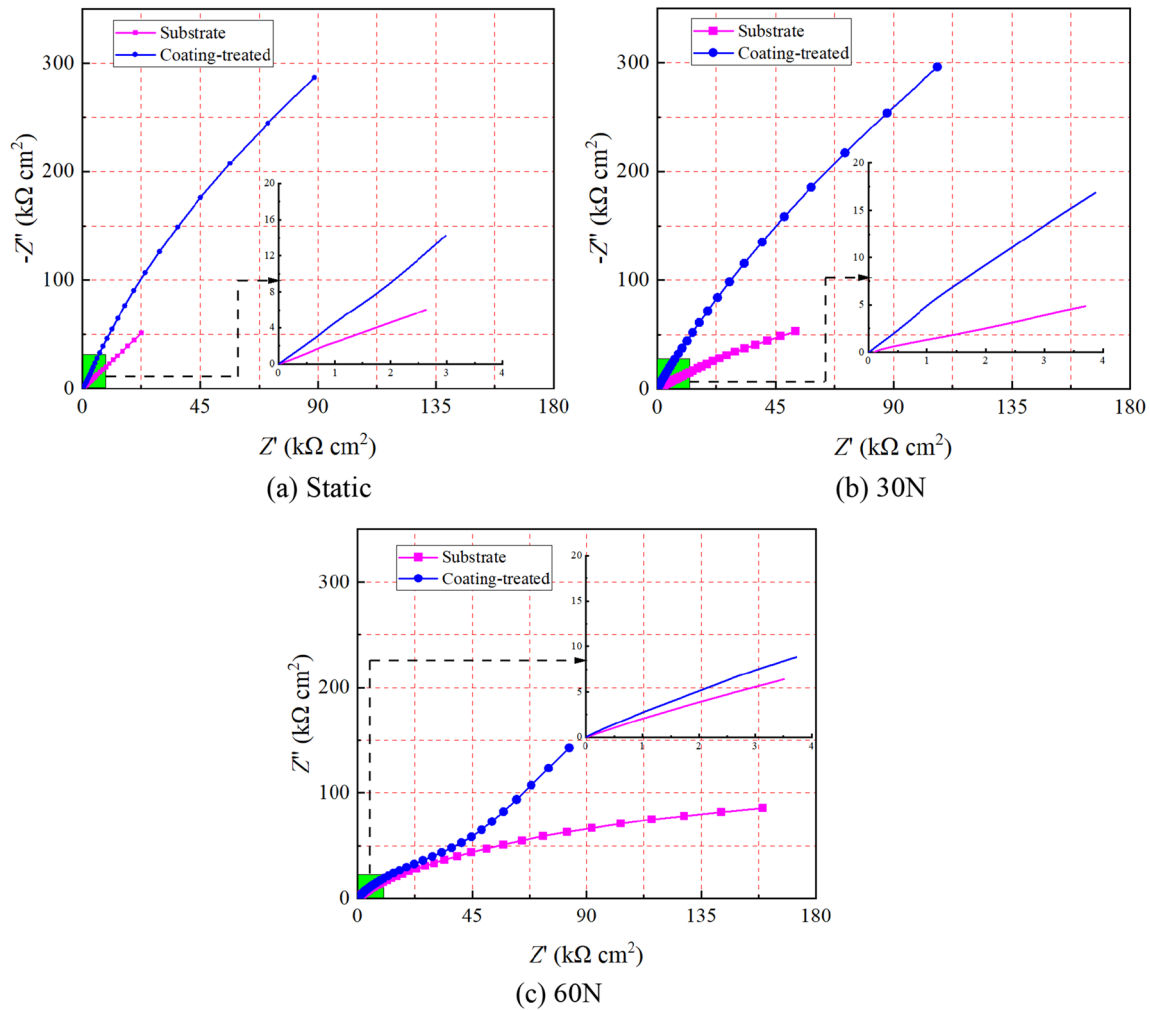


Figure 11 Nyquist plots of all test samples.

indicating a typical capacitive performance existed among the tribocorrosion interface. Meanwhile, with the increase in frequency, all impedances tend to nearly approach 0, thus indicating a representative response of solution resistance that delays the processes of charge transfer into lower frequency regions.

The phase angle platform of the coating-treated samples is always wider than that of the substrate alloy tubes, thereby indicating the CrAlTiN coating shows larger resistance of the electrode reaction process and a stronger capacitance response.

Furthermore, the increased normal load would decrease the amplitude of resistance and the frequency range of the high phase angle region caused by enhanced fretting tribocorrosion behavior.

Discussion

In this study, the Abaqus/Explicit finite element package was applied to this analysis attributed to it can well solve nonlinear dynamic problems and recognize the stress–strain change of the alloy tube’s surface when it is subjected to fretting tribocorrosion [36]. Figure 13 shows the fretting wear model, the finite element mesh graph of the tube, and the application condition of normal load and sliding displacement. The sizes of both cylinder and tube are the same as the real experimental test samples. Herein, the cylinder is regarded as a rigid body. The alloy tube is modeled by the J–C models, eight-node brick hexahedral elements with reduced integration and hourglass control (C3D8R) are applied to realize finite element grid division. Moreover, the meshes in the wear contact area are much finer than other areas

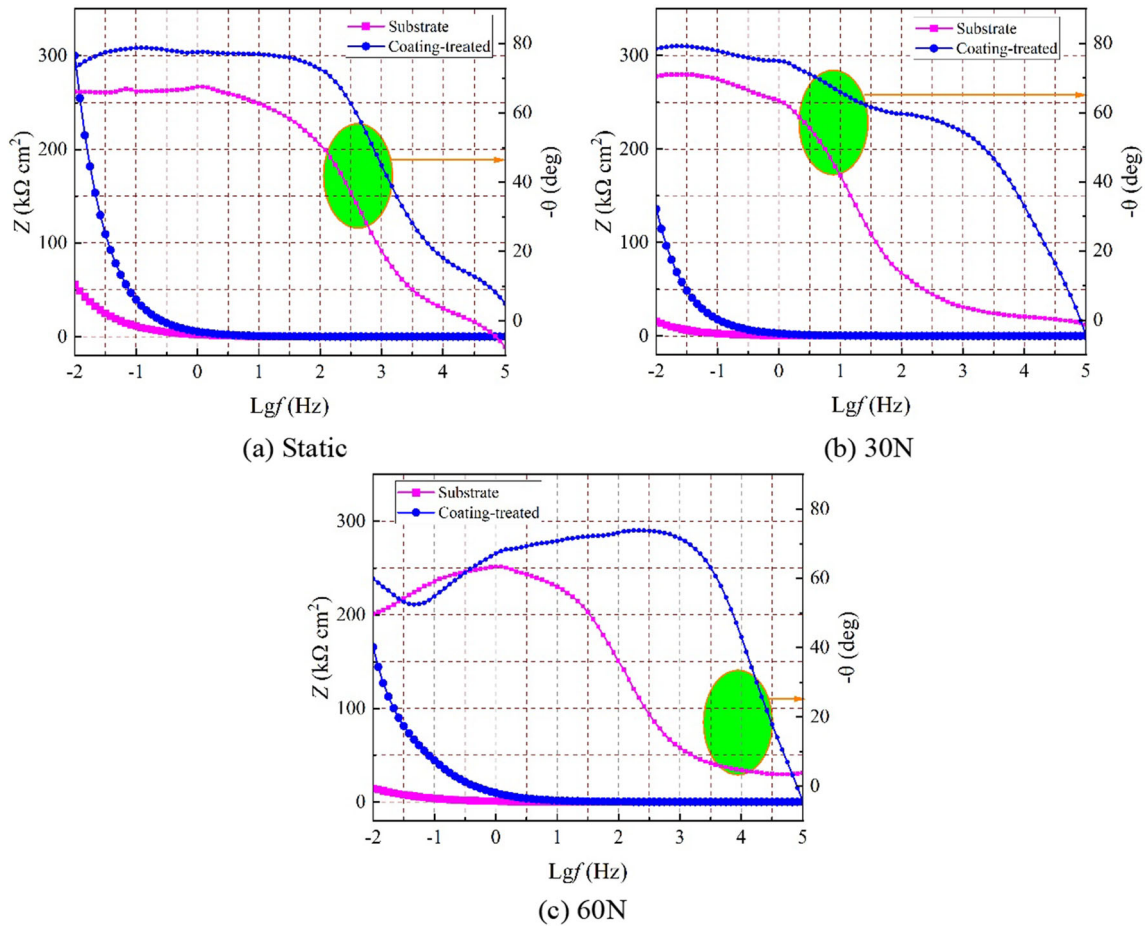


Figure 12 Tafel plots of all test samples.

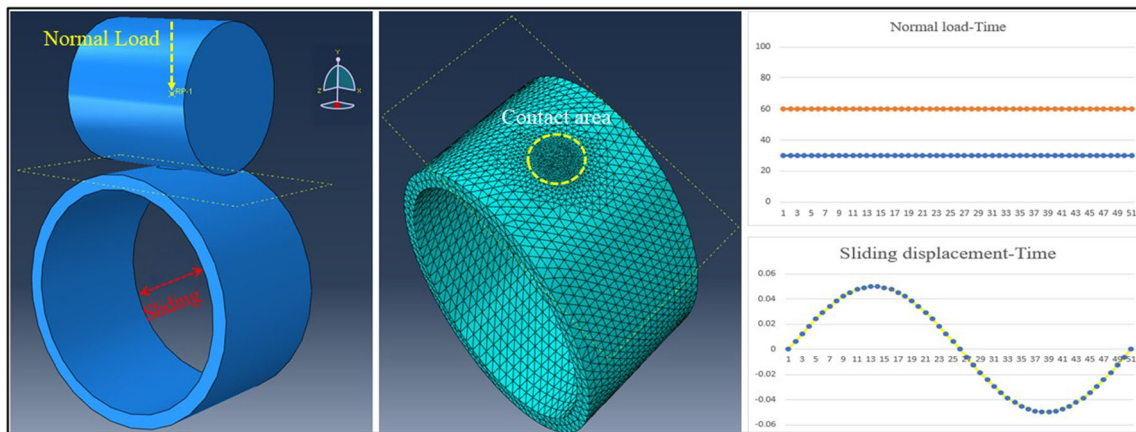


Figure 13 Diagram of numerical simulation.

to enable a more precise analysis of the fretting stress and strain. Table 2 exhibits the mechanical property parameters of all simulated materials and the interfacial friction coefficient of various fretting conditions.

Furthermore, the alloy tube here was assumed to be isotropic, linear elastic, and following the von Mises yield criterion. However, only one fretting cycle was analyzed here; hence, only elastic deformation occurred on the fretting surface. In addition,

Table 2 Some mechanical properties of test samples

Test sample	Mass density (g/cm ³)	Young’s modulus (GPa)	Poisson’s ratio	Friction coefficient	
				30 N	60 N
Substrate	8.19	211.15	0.289	0.328	0.204
Coating-treated	5.42	279.96	0.30	0.227	0.142
Wear pair	3.50	320.00	0.23		

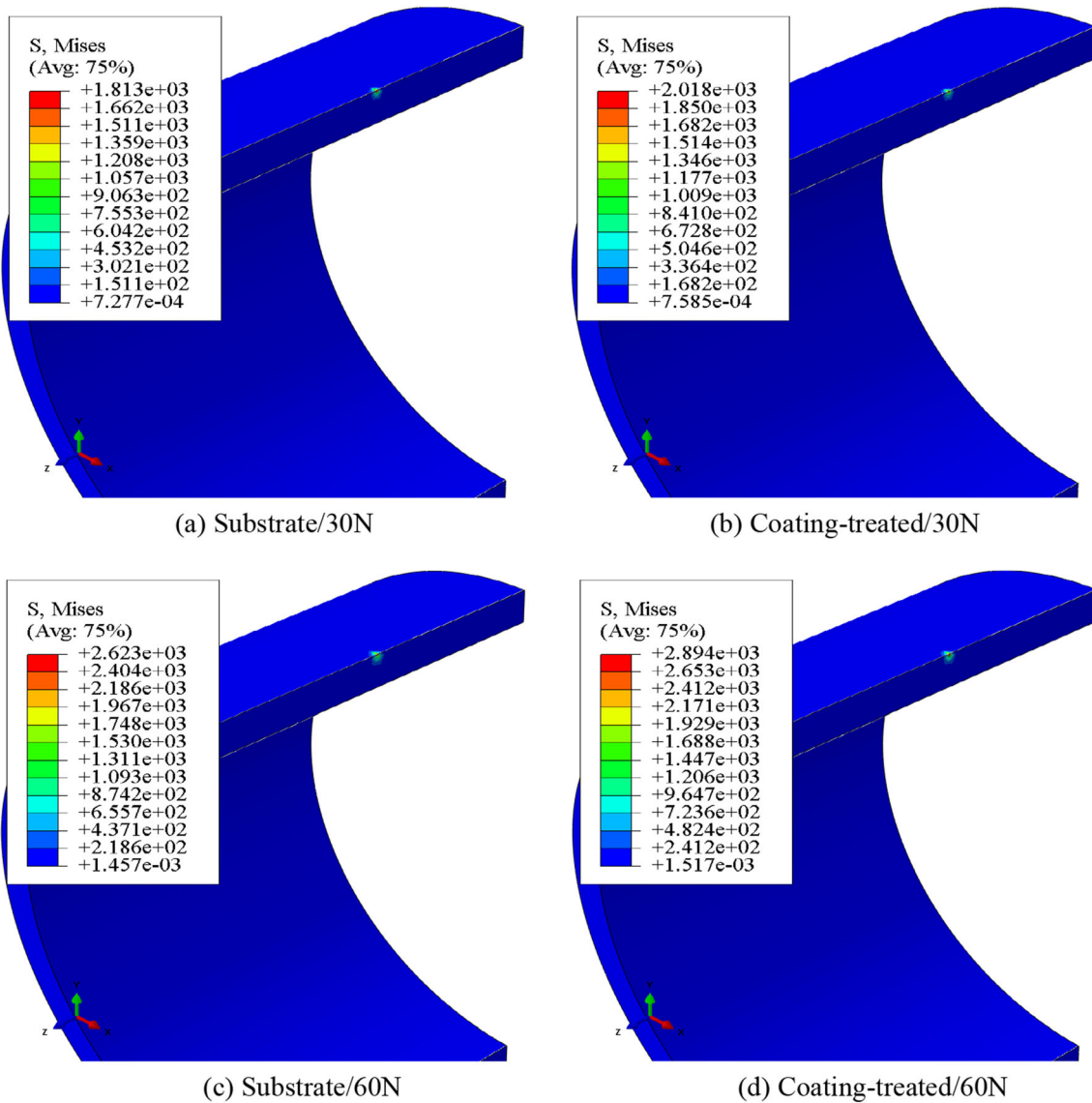


Figure 14 Surface contact stress.

the effect of sea water on the fretting process was ignored. The fretting time was 0.05 s and was the same as that for one cycle of a real experimental test.

Figure 14 shows the maximum stress distribution nephograms of the alloy tube’s interface under

different fretting conditions. When the normal load was 30 N, the maximum contact von Mises stress for the blank and CrAlTiN coating-treated Inconel 690 alloy was approximately 1.813×10^3 and 2.018×10^3 MPa, respectively. Meanwhile, as the

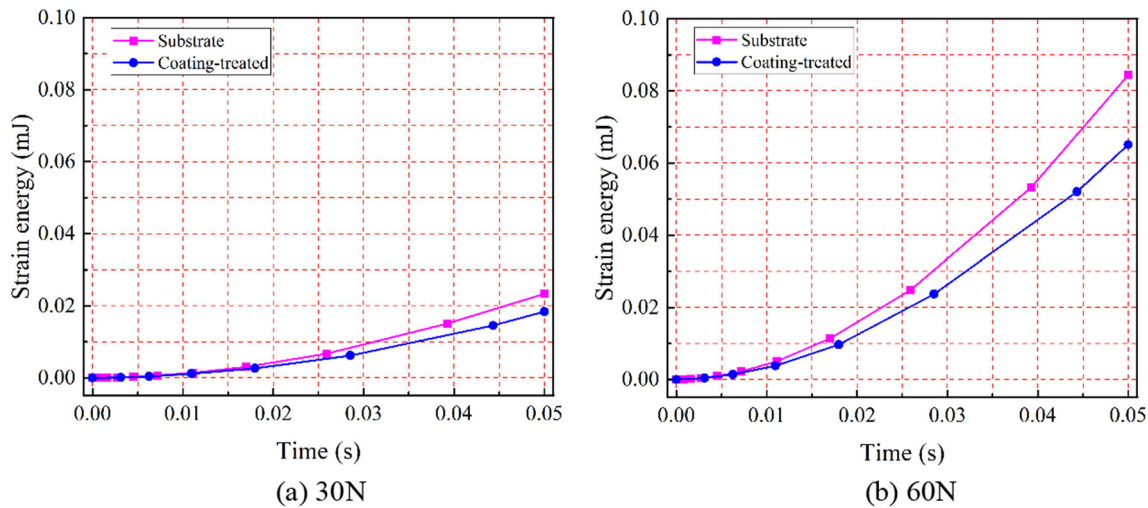


Figure 15 Strain energy of the fretting wear model.

normal load increased to 60 N, the corresponding values increased to 2.623×10^3 and 2.894×10^3 MPa.

It is universally acknowledged that contact stress is one of the major factors that influence interface wear behavior, and von Mises stress is equivalent to stress for yielding [37]. Herein, the Hertz contact theory was applied to analyze the pressure distribution during the fretting wear contact process. The profile of the cylinder contact with the tube could be reduced to two circles contact, and the maximum contact stress (P_{max}) could be calculated by Eq. (1). Where R_C and R_T are the outer diameters of the Al_2O_3 cylinder and Inconel 690 alloy tube, respectively. The E_r is the effective elastic modulus of the cylinder and tube, which was calculated by Eq. (2) [38]. In general, greater normal force and bigger elastic modulus of the test sample always create greater stress on the contact area. When the normal load was constant, the higher the maximum stress, the effect of strain rate on the dynamic response of the fretting wear interface will be more significant.

Furthermore, high contact stress point is often the weak region that can easily cause micro-crack growth.

$$P_{max} = \frac{1}{\pi} \sqrt{\frac{(R_C + R_T) * E_r * F_N}{R_C R_T}} \quad (1)$$

$$\frac{1}{E_r} = \left(\frac{1 - \epsilon_C^2}{\pi E_C} + \frac{1 - \epsilon_T^2}{\pi E_T} \right) \quad (2)$$

The evolution of strain energy versus fretting time within the entire wear contact process of each test

tube is presented in Fig. 15. Hence, the strain energy was necessary for the material to produce elasto-plastic deformation. During the fretting process, the total strain energy increased with time to a maximum extent. When the normal load was constant, the strain energy of the substrate alloy tube is higher than that of the CrAlTiN coating-treated tube. A higher normal load would increase the strain energy, and the difference between the two was even starker. This indicates that the improvement effect of the Inconel 690 alloy tube's wear resistance is more evident with the increase in normal fretting load.

Conclusions

This study investigated the fretting wear behavior and electrochemical corrosion properties of both blank and CrAlTiN coating-treated Inconel 690 alloy tubes under seawater conditions. Hence, the following conclusions were obtained:

1. The Inconel 690 alloy tube's surface nano-hardness and elastic modulus had been improved distinctly by the CrAlTiN coating, thus helping reduce the volume and depth of worn scars.
2. Considering the compressive residual stress of the CrAlTiN coating surface was poorer than that of the blank alloy tube, the static corrosion resistance of the coating-treated alloy tube was poorer than that of the substrate. However, the coating's better wear resistance could decrease

the removal of materials and further reduce corrosion during the fretting corrosion process.

- An increased normal load increased the tribocorrosion degree, the distinction between the substrate and CrAlTiN coating-treated alloy tube on the wear resistance was becoming more evident in the higher normal load. In addition, the primarily wear mechanisms were abrasive wear and fatigue peeling.

Acknowledgements

Thanks to Mr. Hui Qiu and Xiaohui Kang, Professor Meigui Yin and Guizhong Li of Wenzhou University.

Authors' contributions

XK writing and editing this manuscript; HQ reviewing this manuscript; GL provided the test materials and rig; and MY did the experiments, tested, and analyzed all results.

Funding

This work is supported by National Natural Science Foundation of China (No.52105201), Natural Science Foundation of Zhejiang Province, China (Grant No. LQ22E050010).

Data availability

The data that support the findings of this study are available from the corresponding author, upon reasonable request.

Declarations

Conflict of Interest There are no conflicts of interest.

Informed consent Written informed consent for submit this paper was obtained from all authors, and no code of ethics was violated.

References

- Song Q, Liu L, Wen D, Wang Y, Wang G, Yin Z, Wang S (2022) Fretting wear behaviors and mechanism of a high Nb–TiAl alloy with full lamellar microstructure at ambient temperature. *J Mater Sci* 57:15636–15650
- Riznic J (2017) Steam generators for nuclear power plants. Woodhead Publishing
- X.C. Qi (2013) Fretting corrosion behavior of Inconel 690 alloy in seawater and ETA solution. Master Degree. Chengdu, China; Southwest Jiaotong University
- Li J, Yang BB, Lu YH, Xin L, Wang ZH, Shoji T (2017) The effect of normal force on fretting corrosion behavior of Inconel 690 in 3.5% sodium chloride. *Mater. Charact.* 131:224–233
- Liao JP, Wu XQ, Tan JB, Tang LC, Qian H, Xie YC (2018) Fretting corrosion fatigue of Alloy 690 in high-temperature pure water. *Corros Sci* 133:423–431
- Zhang YS, Ming HL, Tang LC, Wang JQ, Qian H, Han EH (2021) Effect of the frequency on fretting corrosion behavior between Alloy 690TT tube and 405 stainless steel plate in high temperature pressurized water. *Tribol Int* 164:107229
- Xin L, Lu YH, Otsuka Y, Mutoh Y, Wang ZH, Shoji T (2017) The role of frequency on fretting corrosion of Alloy 690TT against 304 stainless steel in high temperature high pressure water. *Mater Charact* 134:260–273
- Xin L, Yang BB, Li J, Lu YH, Shoji T (2017) Microstructural characteristics of Alloy 690TT subjected to fretting corrosion in high temperature water. *Corros Sci* 123:116–128
- Liu XC, Ming HL, Zhang ZM, Wang JQ, Tang LC, Qian H, Xie YC, Han EH (2019) Effects of temperature on fretting corrosion between alloy 690TT and 405 stainless steel in pure water. *Acta Metall Sin* 32:1437–1448
- Lister DH, Féron D (2012) Nuclear corrosion science and engineering. Elsevier, Amsterdam
- Xin L, Han YM, Ling LG, Lu YH, Shoji T (2020) Effects of dissolved oxygen on partial slip fretting corrosion of Alloy 690TT in high temperature pure water. *J Nucl Materials* 542:152483
- Lee YB, Jeon SH, Bae BJ, Hur DH, Lee JH (2022) Effect of organic film on magnetite deposition behavior of alloy 690 steam generator tubes in simulated PWR secondary system. *J Mater Res Tech* 20:2527–2541
- Kontou A, Taylor RI, Spikes HA (2021) Effects of dispersant and ZDDP additives on fretting wear. *Tribol Lett* 69:1–13
- Hou Q, Liu ZY, Li CT, Li XG, Shao JM (2019) Degradation of the oxide film formed on alloy 690TT in a high-temperature chloride solution. *Appl Surf Sci* 467:1104–1112

- [15] Diercks DR, Shack WJ, Muscara J (1999) Overview of steam generator tube degradation and integrity issues. *Nucl Eng Des* 194:19–30
- [16] Kelly RG, Scully JR, Shoosmith D, Buchheit RG (2002) *Electrochemical techniques in corrosion science and engineering*. CRC Press
- [17] Persaud SY, Carcea AG, Newman RC (2015) An electrochemical study assisting the interpretation of acid sulfate stress corrosion cracking of NiCrFe alloys. *Corros Sci* 90:383–391
- [18] Betova I, Bojinov M, Ikäläinen T, Saario T, Sipilä K (2022) Corrosion of alloy 690 in simulated steam generator crevices: effect of applied potential, pH and Pb addition. *J Electrochem Soc* 169:021502
- [19] Wang JZ, Wang JQ, Ming HL, Zhang ZM, Han EH (2018) Effect of temperature on corrosion behavior of alloy 690 in high temperature hydrogenated water. *J Mater Sci Technol* 34:1419–1427
- [20] Li XX, Liu J, Liu JB, Zhu SJ, Yan YX, Zhang XH, Liang TX (2021) Corrosion behaviour of nanocrystalline alloy 690 at high-temperature and high-pressure in simulated PWR secondary environment. *Surf Topogr-Metrol* 9:015006
- [21] Euch SE, Bricault D, Cachet H, Sutter EM, Tran MT, Vivier V, Engler N, Marion A, Skocic M, Huerta-Ortega B (2019) Temperature dependence of the electrochemical behavior of the 690 Ni-base alloy between 25 and 325 °C. *Electrochim Acta* 317:509–520
- [22] Liu J, Liu JB, Zhang XH, Ahmad T, Liang TX, Zeng LF, Wang CM, Yang B (2020) Effect of ultrasonic surface rolling treatment on corrosion behavior of alloy 690. *Metals* 10:917
- [23] Yin MG, Yin HY, Zhang QQ, Long JQ (2022) Effect of ultrasonic surface rolling process on the high temperature fretting wear behavior of Inconel 690 alloy. *Wear* 500:204347
- [24] Maleki E, Unal O (2021) Optimization of shot peening effective parameters on surface hardness improvement. *Met Mater Int* 27:3173–3185
- [25] Lee TH, Suh HY, Han SK, Noh JS, Lee JH (2016) Effect of a heat treatment on the precipitation behavior and tensile properties of alloy 690 steam generator tubes. *J Nucl Mater* 479:85–92
- [26] Maher I, Mehran QM (2022) Adhesion strength prediction of CrAlN coating on Al–Si alloy (LM28): fuzzy modelling. *Met Mater Int* 28:421–432
- [27] Yang Q, McKellar R (2015) Nanolayered CrAlTiN and multilayered CrAlTiN–AlTiN coatings for solid particle erosion protection. *Tribol Int* 83:12–20
- [28] Chen JH, Guo QQ, Li JP, Yang Z, Guo YC, Yang W, Xu DP, Yang B (2022) Microstructure and tribological properties of CrAlTiN coating deposited via multi-arc ion plating. *Mater Today Commun* 30:103136
- [29] Haglöf F, Kaplan B, Norgren S, Blomqvist A, Selleby M (2019) Experimental study of carbides in the Ti–Cr–C system. *J Mater Sci* 54:12358–12370
- [30] Bijalwan P, Kumar A, Nayak SK, Banerjee A, Dutta M, Laha T (2019) Microstructure and corrosion behavior of Fe-based amorphous composite coatings developed by atmospheric plasma spraying. *J Alloy Compd* 796:47–54
- [31] Fanicchia F, Maeder X, Ast J, Taylor AA, Guo Y, Polyakov MN, Michler J, Axinte DA (2018) Residual stress and adhesion of thermal spray coatings: Microscopic view by solidification and crystallisation analysis in the epitaxial CoNiCrAlY single splat. *Mater Design* 153:36–46
- [32] Danek M, Fernandes F, Cavaleiro A, Polcar T (2017) Influence of Cr additions on the structure and oxidation resistance of multilayered TiAlCrN films. *Surf Coat Tech* 313:158–167
- [33] Li J, Yang BB, Lu YH, Xin L, Wang ZH, Shoji T (2017) The effects of electrochemical polarization condition and applied potential on tribocorrosion behaviors of Inconel 690 alloys in water environment. *Mater Design* 119:93–103
- [34] Yan SK, Song GL, Li ZX, Wang HN, Zheng DJ, Cao FY, Horynova M, Dargusch MS, Zhou L (2018) A state-of-the-art review on passivation and biofouling of Ti and its alloys in marine environments. *J Mater Sci Technol* 34:421–435
- [35] Mousavi SE, Naghshehkish N, Amirnejad M, Shammakhi H, Sonboli A (2021) Wear and corrosion properties of stellite-6 coating fabricated by HVOF on nickel–aluminium bronze substrate. *Met Mat Int* 27:3269–3281
- [36] Siswanto WA, Nagentrau M, Mohd Tobi AL, Tamin MN (2016) Prediction of plastic deformation under contact condition by quasi-static and dynamic simulations using explicit finite element analysis. *J. Mech. Sci. Technol.* 30:5093–5101
- [37] Stronge WJ (2018) *Impact mechanics*. Cambridge University Press
- [38] Johnson KL (1987) *Contact mechanics*. Cambridge University Press

Publisher's Note Springer Nature remains neutral with regard to jurisdictional claims in published maps and institutional affiliations.

Springer Nature or its licensor (e.g. a society or other partner) holds exclusive rights to this article under a publishing agreement with the author(s) or other rightsholder(s); author self-archiving of the accepted manuscript version of this article is solely governed by the terms of such publishing agreement and applicable law.